

The magnetic helicity density patterns from non-axisymmetric solar dynamo

Valery V. Pipin

Institute for Solar-Terrestrial Physics, PO Box 291, Lermontov st., 126a, Irkutsk, 664033, Russia

(Received xx; revised xx; accepted xx)

In the paper, we study the helicity density patterns which can result from the emerging bipolar regions. Using the relevant dynamo model and the magnetic helicity conservation law we find that the helicity density pattern around the bipolar regions depends on the configuration of the ambient large-scale magnetic field, and in general, they show the quadrupole distribution. The position of this pattern relative to the equator can depend on the tilt of the bipolar region. We compute the time-latitude diagrams of the helicity density evolution. The longitudinally averaged effect of the bipolar regions shows two bands of sign for the density distribution in each hemisphere. Similar helicity density patterns are provided by the helicity density flux from the emerging bipolar regions subjected to the surface differential rotation.

1. Introduction

The magnetic helicity conservation is often considered as one of the most important ingredient in the magnetic field generation on the Sun and other solar type stars (Brandenburg & Subramanian 2005; Blackman & Thomas 2015). It is also important for the magnetic activities in the solar atmosphere and corona (Mackay & Yeates 2012). The magnetic helicity characterizes the complexity of the magnetic field topology in the closed volume (Berger 1984). Observing the magnetic field on the surface we can deduce some local proxies of the helicity integral. The observational constraints of the solar dynamo models are related to the hemispheric helicity rules (Seehafer 1994; Pevtsov *et al.* 1994) and the magnetic helicity fluxes from the solar interior (Berger & Ruzmaikin 2000; Blackman & Brandenburg 2003). The hemispheric helicity rule (hereafter HHR) follows from the theoretical properties of the large-scale dynamo which we expect to be working in the solar interior. This rule states that the small-scale magnetic fields on the northern hemisphere have the negative twist (the right-hand coordinate system) and the opposite twist is in the southern hemisphere. In the dynamo theory the small scales include scale of the solar active regions and smaller ones. The helicity conservation constrains the helicity sign distribution over the spatial scales. The results of Pouquet *et al.* (1975) showed that in the turbulent dynamo processes we can expect that the twist of the large-scale magnetic field is opposite to the twist of the small-scale magnetic field. This property is also called the bi-helical dynamo.

The vector magnetic field observations make possible to deduce the information about the magnetic and current helicity density on the solar surface (Pevtsov *et al.* 1994; Bao & Zhang 1998; Zhang *et al.* 2010). In general, these proxies show the HHR for the small-scale magnetic field. The issues about the HHR of the large-scale magnetic field and the bi-helical solar dynamo are still debatable (Brandenburg *et al.* 2017; Singh *et al.* 2018; Pipin *et al.* 2019).

However, the relevance of the local proxies, which are observed on the surface, as the

proxies of the bi-helical magnetic fields generated by the dynamo processes in the depth of the convection zone can be questioned. On the surface some of the helical magnetic field configurations can be generated by means of other processes which are not readily related to the dynamo. For example, the emerging of the magnetic field on the surface and its interaction with the ambient magnetic field can produce the local helicity flux. Hawkes & Yeates (2019) showed one of such example, see Fig4c in their paper. They illustrated that the emerging bipolar region which interacts with the global magnetic field results to the local quadrupole helicity density flux pattern. Interesting that this effect drives the helicity density flux butterfly diagrams, which are satisfying the own HHR, see the Fig3c in their paper. Another kind of this effect was illustrated by Pipin *et al.* (2019) in their benchmark dynamo model. Here we elaborate on this example and study the effect of the emerging bipolar regions on the surface helicity density patterns. Note, on the solar surface the most magnetic activity is produced by the sunspots (Stenflo 2013). We find that the emerging active regions can bias our conclusions about the helical properties of the dynamo inside the convection zone. The study is based on the numerical simulations of the nonaxisymmetric dynamo model, which was suggested recently by Pipin & Kosovichev (2018). The next section describes the model.

2. Dynamo model

Evolution of the large-scale magnetic field in perfectly conductive media is described by the mean-field induction equation (Krause & Rädler 1980):

$$\partial_t \langle \mathbf{B} \rangle = \nabla \times (\mathcal{E} + \langle \mathbf{U} \rangle \times \langle \mathbf{B} \rangle) \quad (2.1)$$

where $\mathcal{E} = \langle \mathbf{u} \times \mathbf{b} \rangle$ is the mean electromotive force; \mathbf{u} and \mathbf{b} are the turbulent fluctuating velocity and magnetic field respectively; and $\langle \mathbf{U} \rangle$ and $\langle \mathbf{B} \rangle$ are the mean velocity and magnetic field. Pipin & Kosovichev (2018) (PK18) suggested the minimal set of the dynamo equations to model the nonaxisymmetric magnetic field evolution. In this model, similarly to Moss *et al.* (2008), we neglect the radial dependence of magnetic field, and assume that the radial gradient of angular velocity is greater than the latitudinal gradient. In earlier studies, e.g., Jennings *et al.* (1990) it was found that neglecting of terms related to r-dependence may cause significant reduction of the threshold for magnetic field excitation by a dynamo process. By this reason, we construct our model in such a way that it holds the results of Moss *et al.* (2008) in the limit of the axisymmetric 1D case. Therefore the results of the model pertain to the illustrative character which is typical for the 1D toy dynamo models.

It is convenient to represent the vector $\langle \mathbf{B} \rangle$ in terms of the axisymmetric and nonaxisymmetric components as follows:

$$\langle \mathbf{B} \rangle = \bar{\mathbf{B}} + \tilde{\mathbf{B}} \quad (2.2)$$

$$\bar{\mathbf{B}} = \hat{\phi} B + \nabla \times (A \hat{\phi}) \quad (2.3)$$

$$\tilde{\mathbf{B}} = \nabla \times (\mathbf{r}T) + \nabla \times \nabla \times (\mathbf{r}S), \quad (2.4)$$

where $\bar{\mathbf{B}}$ and $\tilde{\mathbf{B}}$ are the axisymmetric and nonaxisymmetric components; A , B , T and S are scalar functions representing the field components; $\hat{\phi}$ is the azimuthal unit vector, \mathbf{r} is the radius vector; r is the radial distance, and θ is the polar angle. Besides, we apply the following gauge (see, e.g., Krause & Rädler 1980):

$$\int_0^{2\pi} \int_{-1}^1 S d\mu d\phi = \int_0^{2\pi} \int_{-1}^1 T d\mu d\phi = 0, \quad (2.5)$$

using this gauge we exclude contributions from gradient of the scalar functions in definitions of T and S . The magnetic helicity determined in such a way is called the “absolute” measure of helicity (Berger & Hornig 2018).

Hereafter, the over-bar denotes the axisymmetric magnetic field, and tilde denotes non-axisymmetric properties. Following the above ideas we consider a reduced dynamo model where we neglect the radial dependence of the magnetic field. In this case, the induction vector of the large-scale magnetic field is represented in terms of the scalar functions as follows:

$$\begin{aligned} \langle \mathbf{B} \rangle = & -\frac{\mathbf{r}}{R^2} \frac{\partial \sin \theta A}{\partial \mu} - \frac{\hat{\theta}}{R} A + \hat{\phi} B \\ & - \frac{\mathbf{r}}{R^2} \Delta_{\Omega} S + \frac{\hat{\theta}}{\sin \theta} \frac{\partial T}{\partial \phi} + \hat{\phi} \sin \theta \frac{\partial T}{\partial \mu}, \end{aligned} \quad (2.6)$$

where R represents the radius of the spherical surface inside a star where the hydromagnetic dynamo operates. The above equation defines the 3d divergence free B-field on the sphere. In the model we employ the simple expression of \mathcal{E} :

$$\mathcal{E} = \alpha \langle \mathbf{B} \rangle - \eta_T \nabla \times \langle \mathbf{B} \rangle + V_{\beta} \hat{\mathbf{r}} \times \langle \mathbf{B} \rangle + \alpha_{\beta} \hat{\phi} \langle \mathbf{B} \rangle_{\phi} \quad (2.7)$$

The last term is introduced to simulated the tilt of the emerging active regions. The magnetic buoyancy is source of the non-axisymmetric magnetic field in the model. We assume that the magnetic buoyancy acts on relatively small-scale parts of the axisymmetric magnetic field, perhaps, it is caused by some kind of nonlinear instability. It is formulated as following:

$$\begin{aligned} V_{\beta} = & \frac{\alpha_{\text{MLT}}}{\gamma} u_c \beta^2 K(\beta) (1 + \xi_{\beta}(\phi, \theta)), \beta \geq \beta_{cr} \\ & 0, \beta < \beta_{cr}, \end{aligned} \quad (2.8)$$

where, $\alpha_{\text{MLT}} = 1.9$ is the mixing-length theory parameter, γ is the adiabatic law constant, $\beta = |\langle \mathbf{B} \rangle| / B_{\text{eq}}$, $B_{\text{eq}} = \sqrt{4\pi \bar{\rho} u_c^2}$, function $K(\beta)$ is defined in Kitchatinov & Pipin (1993). For $\beta \ll 1$, we have $K(\beta) \sim 1$, and for the strong magnetic field, when $\beta > 1$, $K(\beta) \sim 1/\beta^3$. The function $\xi_{\beta}(\phi, \theta)$ describes the latitudinal and longitudinal dependence of the instability, and parameter β_{cr} controls the instability threshold. In this formulation, the preferable latitude of the “active region emergence” is determined by the latitude of the maximum of the toroidal magnetic field energy, θ_{max} . The magnetic buoyancy instability perturbations are determined by function:

$$\xi_{\beta}(\phi, \theta) = C_{\beta} \exp \left(-m_{\beta} \left(\sin^2 \left(\frac{\phi - \phi_0}{2} \right) + \sin^2 \left(\frac{\theta - \theta_{\text{max}}}{2} \right) \right) \right), \quad (2.9)$$

The instability is randomly initiated in the northern or southern hemispheres, and the longitude, ϕ_0 , is also chosen randomly. We arbitrary chose the fluctuation interval $\tau_{\beta} = 0.01 P_{\text{cyc}}$, where P_{cyc} is the dynamo cycle period. The dynamic of the buoyancy instability is restricted by the five time run-steps. In the model we measure the time in the diffusive units, R^2/η_T . If we scale the dynamo period of the model to 11 years, then the simulated emerging time is about one week, which is much longer than on the Sun (Toriumi & Wang 2019). Parameter m_{β} controls the spatial scale of the instability. Theoretically, using a high values of m we can reproduce the spatial scale of the solar active regions. However, this requires increasing the resolution in both longitude

and latitude, and becomes computationally expensive. We chose the value $m_\beta = 100$, which allows us to accurately resolve the evolving nonaxisymmetric perturbations of magnetic field, and qualitatively reproduce the essential physical effects. Parameter C_β controls the amount of the injected magnetic flux. If large-scale toroidal magnetic flux at a given co-latitude θ is transformed into magnetic flux of the perturbation then $\langle \xi_\beta(\phi, t) \rangle_\phi \approx 1$. This condition corresponds to $C_\beta \approx 15$. In reality, solar active regions are formed by concentration of the toroidal magnetic flux emerging in the photosphere. Turbulent convective motions and other physical processes may take part in the process of formation of solar active regions. Therefore, parameter C_β can be higher than the above mentioned value. Similarly to Pipin & Kosovichev (2018), we choose $C_\beta = 40$. In the numerical experiments, we found that higher values of C_β result in strong cycle-to-cycle variability of the magnetic energy even in the case of stationary α -effect. For the chosen C_β , $|\langle \mathbf{B} \rangle| \approx 2 |\overline{B}_\phi|$, therefore fluctuations of the magnetic field because of the magnetic buoyancy instability are of the order of the axisymmetric toroidal magnetic field strength, which is widely accepted in the literature (Krause & Rädler 1980; Brandenburg & Subramanian 2005).

In the model the strength of the magnetic field is measured relative to the strength of the equipartition field, B_{eq} . Dependence of the instability on the toroidal magnetic field strength results in the magnetic cycle modulation in the number of the bipolar regions. Besides, the critical parameter $\beta_{\text{cr}} = 0.5$ prevents the emergence of active regions at high latitudes. To get the model closer to observations the temporal and spatial resolution have to be increased. Bearing in mind the whole simplicity of our model we restrict ourselves to the qualitative considerations. In our description, the magnetic buoyancy instability results in generation of the non-axisymmetric magnetic field in form of the magnetic bipolar regions. Besides, it results in the magnetic flux loss and the large-scale dynamo saturation for the magnetic field strength $|\mathbf{B}| > 0.5B_{\text{eq}}$. This was anticipated earlier by Parker (1984); Noyes *et al.* (1984). despite it is restricted to the non-axisymmetric magnetic field

In this paper we would to calculate the magnetic helicity flux provided by emergence of the tilted active regions on the solar surface. For this purpose, we assume that the emerging due to magnetic instability part of the toroidal magnetic field is subjected to some extra α effect, which is caused by the dynamic of the magnetic loop. Note, that the dynamic of the buoyancy instability is restricted to 5 time run-steps. With this choice, we find that a 5° tilt (Tlatov *et al.* 2013) can be reproduced if we put

$$\alpha_\beta = \frac{1}{3} \cos \theta V_\beta, \quad (2.10)$$

where V_β is determined by the Eq(2.8) and the coefficient $1/3$ was found by the numerical experiments. In case of $\alpha_\beta = V_\beta$ the tilt is around $\pi/4$. Note, that the first term in the equation (2.7) includes the α -effect which acts on the unstable part of the nonaxisymmetric magnetic field and produces some amount of tilt as well. We find this effect negligible in comparison observations. We deliberately assume that the α_β -effect acts only on the nonaxisymmetric part of the magnetic field. In this case, it does not change the conditions for the linear stability of the axisymmetric magnetic field.

For the standard part of α effect we use the phenomenological description and take into account the contribution of the magnetic helicity in following to suggestions of Pouquet *et al.* (1975):

$$\alpha = \alpha_0 \cos \theta + \frac{\langle \mathbf{b} \cdot \nabla \times \mathbf{b} \rangle \tau_c}{4\pi\bar{\rho}} \quad (2.11)$$

where α_0 is a free positive parameter which controls the strength of the α -effect. The results of the above-cited paper suggest that the negative sign of the small-scale current helicity results from the magnetic helicity conservation. In following to Moffatt (1978) we replace $\langle \mathbf{b} \cdot \nabla \times \mathbf{b} \rangle \sim \langle \chi \rangle / \ell^2$, where $\langle \chi \rangle$ is the magnetic helicity density, $\langle \chi \rangle = \langle \mathbf{a} \cdot \mathbf{b} \rangle$ (\mathbf{a} and \mathbf{b} are the fluctuating parts of magnetic field vector-potential and magnetic field vector). The magnetic helicity conservation results to the dynamical quenching of the dynamo (Kleeorin & Ruzmaikin 1982; Kleeorin & Rogachevskii 1999; Kleeorin *et al.* 2000). For the sake of simplicity, the above equation (2.10) has no explicit inclusion of magnetic helicity. It is partly justified by the fact that in our formulation the α_β term is not a primary dynamo effect. This is in contrast with the Babcock-Leighton scenario for the solar dynamo (Charbonneau 2011). In following to Blackman & Brandenburg (2003), we can anticipate that the explicit addition of the magnetic helicity term in the equation (2.10) will result in a reduction of the bipolar region tilt. Also, in our we do not include any algebraic quenching (see, Ruediger & Kichatinov 1993) in the α -effect contributions in Eq(2.10) and Eq(2.11). For a simple plane model like ours, the only result of the algebraic α -quenching is the reduction of the magnitude of the generated toroidal magnetic field. We find that the model reproduces the finite-amplitude dynamo waves of the reference model of Moss *et al.* (2008) even for the case when we have the only nonlinear effect due to the magnetic buoyancy term. Therefore, we skip the algebraic α -quenching in our calculations.

Similarly to Hubbard & Brandenburg (2012); Pipin *et al.* (2013); Brandenburg (2018), in our model we use the global conservation law for the total magnetic helicity. In this case the magnetic helicity density, $\langle \chi \rangle = \langle \mathbf{a} \cdot \mathbf{b} \rangle$, is governed by the equation:

$$\left(\frac{\partial}{\partial t} + \langle \mathbf{U} \rangle \cdot \nabla \right) \langle \chi \rangle^{(tot)} = - \frac{\langle \chi \rangle}{R_m \tau_c} - 2\eta \langle \mathbf{B} \rangle \cdot \langle \mathbf{J} \rangle - \nabla \cdot \mathcal{F}^\chi, \quad (2.12)$$

where $\langle \chi \rangle^{(tot)} = \langle \chi \rangle + \langle \mathbf{A} \rangle \cdot \langle \mathbf{B} \rangle$ is the total magnetic helicity density of the mean and turbulent fields. It is assumed that $\nabla \cdot \langle \mathbf{U} \rangle = 0$. Note, that in derivations of the Eq.(2.12), in following Kleeorin & Rogachevskii (1999), we have $2\eta \langle \mathbf{b} \cdot \mathbf{j} \rangle = \frac{\langle \chi \rangle}{R_m \tau_c}$. The $\mathcal{F}^\chi = -\eta_\chi \nabla \langle \chi \rangle^{(tot)}$ is the diffusive flux of the total magnetic helicity, and R_m is the magnetic Reynolds number. The coefficient of the turbulent helicity diffusivity, η_χ , is chosen ten times smaller than the isotropic part of the magnetic diffusivity (Mitra *et al.* 2010): $\eta_\chi = \frac{1}{10} \eta_T$. Here, in comparison to the axisymmetric model of Pipin *et al.* (2013), we have to take into account the redistribution of the nonaxisymmetric part magnetic helicity by the differential rotation. Our ansatz differs from that suggested by papers of Kleeorin & Ruzmaikin (1982); Kleeorin & Rogachevskii (1999). Here, the turbulent fluxes of the magnetic helicity are approximated by the only term which is related to the diffusive flux. Pipin *et al.* (2013) found that the dynamo models, where helicity evolution follows the Eq(2.12), show a magnetic helicity wave propagating with the dynamo wave. This alleviates the so-called catastrophic quenching of the α -effect (Brandenburg 2018).

Similarly to the magnetic field, the mean magnetic helicity density can be formally decomposed into the axisymmetric and non-axisymmetric parts: $\langle \chi \rangle^{(tot)} = \bar{\chi}^{(tot)} + \tilde{\chi}^{(tot)}$. The same can be done for the magnetic helicity density of the turbulent field: $\langle \chi \rangle = \bar{\chi} + \tilde{\chi}$, where $\bar{\chi} = \overline{\mathbf{a} \cdot \mathbf{b}}$ and $\tilde{\chi} = \langle \mathbf{a} \cdot \mathbf{b} \rangle$. Then we have,

$$\bar{\chi}^{(tot)} = \bar{\chi} + \overline{\mathbf{A} \cdot \mathbf{B}} + \overline{\tilde{\mathbf{A}} \cdot \tilde{\mathbf{B}}}, \quad (2.13)$$

$$\tilde{\chi}^{(tot)} = \tilde{\chi} + \overline{\mathbf{A} \cdot \tilde{\mathbf{B}}} + \overline{\tilde{\mathbf{A}} \cdot \mathbf{B}} + \overline{\tilde{\mathbf{A}} \cdot \tilde{\mathbf{B}}}, \quad (2.14)$$

Evolution of the $\bar{\chi}$ and $\tilde{\chi}$ is governed by the corresponding parts of Eq(2.12). Thus,

the model takes into account contributions of the axisymmetric and nonaxisymmetric magnetic fields in the whole magnetic helicity density balance, providing a non-linear coupling. We see that the α -effect is dynamically linked to the longitudinally averaged magnetic helicity of the $\tilde{\mathbf{B}}$ -field, which is the last term in Eq(2.13). Thus, the nonlinear α -effect is *non-axisymmetric*, and it contributes into coupling between the $\bar{\mathbf{B}}$ and $\tilde{\mathbf{B}}$ modes. The coupling works in both directions. For instance, the azimuthal α -effect results in $\mathcal{E}_\phi = \alpha \langle B_\phi \rangle + \alpha_\beta \tilde{B}_\phi$. If we denote the nonaxisymmetric part of the α by $\tilde{\alpha}$ then the mean electromotive force is $\bar{\mathcal{E}}_\phi = \bar{\alpha} \bar{B}_\phi + \tilde{\alpha} \tilde{B}_\phi + \alpha_\beta \tilde{B}_\phi$. This introduces a new generation source which is usually ignored in the axisymmetric dynamo models. The magnetic helicity conservation is determined by the magnetic Reynolds number R_m . In this paper we employ $R_m = 10^6$.

The helicity conservation in form the Eq.(2.12) is suitable for the dynamo simulation. To estimate the helicity flux from the dynamo we will follow the approach of Berger & Ruzmaikin (2000). We derive the equation for the small-scale helicity integral in Appendix 5.3. The change of the helicity integral is determined by the the dynamo processes inside and the helicity fluxes out of the dynamo regions as follows,

$$\begin{aligned} \left(\frac{d}{dt} + \frac{1}{R_m \tau_c} \right) \int \langle \chi \rangle dV &= -2 \int \mathcal{E} \cdot \langle \mathbf{B} \rangle dV - \int \mathcal{F}^\chi \cdot \mathbf{n} dS \\ &- 2 \oint (\langle \mathbf{A} \rangle \cdot \langle \mathbf{U} \rangle) (\langle \mathbf{B} \rangle \cdot \mathbf{n}) dS - 2 \oint (\mathcal{E} \times \langle \mathbf{A} \rangle) \cdot \mathbf{n} dS \\ &- 2\eta \oint (\langle \mathbf{A} \rangle \times \langle \mathbf{J} \rangle) \cdot \mathbf{n} dS + \oint (\langle \mathbf{A} \rangle \cdot \langle \mathbf{B} \rangle) (\langle \mathbf{U} \rangle \cdot \mathbf{n}) dS \end{aligned} \quad (2.15)$$

This equation is compatible with the Eq(2.12). The latter is solved in our simulations. We use the right hand parts of Eq.(2.15) to estimate the helicity density fluxes and their integral. The first term in the second line of the equation (2.15) defines the helicity flux due to the differential rotation. The corresponding helicity density flux:

$$F_\Omega = -2 \langle B_r \rangle \langle A_\phi \rangle \bar{U}_\phi. \quad (2.16)$$

The second term, i.e., $-2 \oint (\mathcal{E} \times \langle \mathbf{A} \rangle) \cdot \mathbf{n} dS$ describes the helicity fluxes due effect of the turbulent flows and magnetic field. The expression of the mean electromotive force contains contributions from the α -effect, turbulent diffusivity and the magnetic buoyancy. For this study we skip the effect of the turbulent diffusivity. Note that this flux is additive to the term in the third line of the Eq(2.15). In our discussion, we leave contributions due to the α and magnetic buoyancy effects:

$$-2 (\mathcal{E} \times \langle \mathbf{A} \rangle) \cdot \mathbf{n} = F_\alpha + F_\beta + \dots, \quad (2.17)$$

$$F_\alpha = -2\alpha (\langle B_\theta \rangle \langle A_\phi \rangle - \langle B_\phi \rangle \langle A_\theta \rangle) + 2\alpha_\beta \langle B_\phi \rangle \langle A_\theta \rangle \quad (2.18)$$

$$F_\beta = 2V_\beta (\langle B_\theta \rangle \langle A_\theta \rangle + \langle B_\phi \rangle \langle A_\phi \rangle) \quad (2.19)$$

Note, that both the axisymmetric and the nonaxisymmetric modes contribute to the all terms in Eq(2.17).

The equations (2.1,2.12) are solved numerically in the non-dimensional form. We assume that the rotational shear is constant in latitude. The effect of differential rotation is controlled by non-dimensional parameter $R_\omega = \frac{R^2}{\eta_T} \frac{\partial \Omega}{\partial r}$, the α -effect is measured by parameter $R_\alpha = \frac{R\alpha_0}{\eta_T}$, the magnetic buoyancy depends on $R_\beta = \frac{R}{\eta_T} \frac{\alpha_{MLT} u_c}{\gamma}$, and

the magnetic field is measured relative to the equipartition strength $B_{eq} = \sqrt{4\pi\bar{\rho}u^2}$. Similarly to Pipin & Kosovichev (2018) we put $R_\omega = \frac{R\Omega}{\eta_T} = 10^3$, $R_\alpha = 1$. This choice describes the $\alpha^2\Omega$ dynamo regime with differential rotation as the main driver of axisymmetric toroidal magnetic field. Note for the given choice of the dynamo parameters the non-axisymmetric modes are stable. They do not take part in the dynamo unless some nonaxisymmetric phenomena come into the play. In this model the non-axisymmetric modes are resulted due to the magnetic buoyancy effect. The R_β controls both the magnetic field strength in bipolar regions and magnetic flux loss. Therefore, it affects the level of the large-scale magnetic field strength in the stationary state. To estimate the magnetic buoyancy parameter we employ results of (Kitchatinov & Pipin 1993) who argued that the maximum buoyancy velocity of large-scale magnetic field of equipartition strength B_{eq} is of the order of 6 m/s. In the solar conditions, the magnetic diffusion $\eta_T = 10^{12}\text{cm}^2/\text{s}$ (Rüdiger *et al.* 2011), and $R_\beta \approx 500$. With this value, we get a very efficient magnetic flux loss, which results in the large-scale toroidal magnetic field strength much less than B_{eq} . This regime is not efficient for the bipolar region production. Hence, we use by an order of magnitude smaller value: $R_\beta = 50$. For this value, we get the “spot’s” magnetic field strength around B_{eq} . Reduction of the R_β to the less values results in the weaker bipolar regions and the stronger larger-scale toroidal magnetic field. Note, that the magnetic helicity in the model is measured in units $B_{eq}^2 R$. Comparing our results with observations, we have to bear in mind that in the model the magnetic field dynamo generation and the bipolar region formation occur in the same place. Therefore the resulted configuration of the axisymmetric magnetic field are expected to be different from the solar surface observation. However, the evolution of the nonaxisymmetric magnetic field mimics the observational magnetic patterns reasonably well (see, Pipin & Kosovichev 2018). The further detail about the model can be found in the above cited paper. Also, the python code for the model can be found at zenodo : Pipin (2018).

3. Results

3.1. Helicity density patterns from bipolar regions

In this section we consider the helicity patterns, which are produced by the emerging bipolar regions. In this case, we start simulations with a simple antisymmetric distribution of the toroidal magnetic field, $\bar{B}_\phi = 2\sin 2\theta$. The two bipolar regions are injected successively in the southern and northern hemispheres with interval about $0.004R^2/\eta_T$. The time in the model is measured in the units of the diffusive time. If we scale the dynamo period of the model to 11 years, then the interval $0.004R^2/\eta_T$ corresponds to 2.5 months.

The Figure 1 illustrates the magnetic field configurations, as well as, the total helicity density, $\mathbf{A} \cdot \mathbf{B} + \hat{\mathbf{A}} \cdot \hat{\mathbf{B}}$, the helicity density of the nonaxisymmetric magnetic fields and the current helicity density distributions, $B_r (\nabla \times \mathbf{B})_r$. The snapshots are taken shortly after formation of the second bipolar region in the northern hemisphere. We see that the helicity density patterns of the bipolar regions have the quadrupole distributions. The large-scale helicity density is in the background. In agreement with the theoretical expectations, the large-scale magnetic field has the positive magnetic and current helicity density sign in the northern hemisphere. This helicity was generated by the large-scale dynamo. The emerging bipolar regions show the inverted quadrupole helicity patterns in the southern and the northern hemispheres. The positive and negative helicity density parts nearly cancel each other in each hemisphere. The effect of tilt most pronounced in

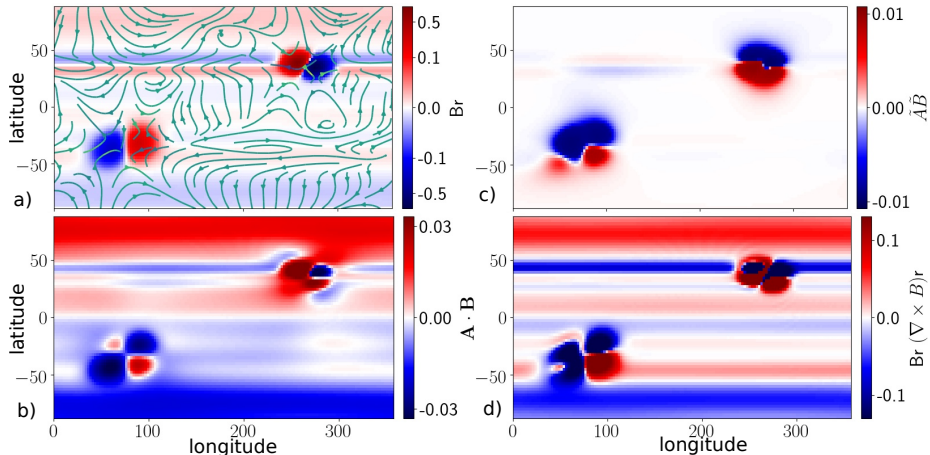


FIGURE 1. a) The color background shows the radial magnetic field (both the axisymmetric and the nonaxisymmetric modes), streamlines show the horizontal non-axisymmetric magnetic field; b) the total magnetic helicity density, $(\bar{\mathbf{A}} + \tilde{\mathbf{A}}) \cdot (\bar{\mathbf{B}} + \tilde{\mathbf{B}})$, c) the same as b) for $\tilde{\mathbf{A}} \cdot \tilde{\mathbf{B}}$; d) the same as b) for the current helicity density.

distribution of the current helicity density. On the $B_r (\nabla \times \mathbf{B})_r$ synoptic map we see the negative trace, which is produced by the emerging region. Therefore, $\tilde{B}_r (\nabla \times \tilde{\mathbf{B}})_r < 0$ inside the latitudinal band of the bipolar region. We did not find this effect in another run where we neglect the α_β term in the mean electromotive force. Also, some part of the net helicity is due to participation of the bipolar regions in the large-scale dynamo.

The Figure 2 illustrates the patterns of the helicity density fluxes, the terms, F_Ω , F_α and F_β in the Eq(2.15) for the models with and without tilt effect. We find that coupling the emerging bipolar regions and the differential rotation produces the flux pattern which is inverted to the helicity density, $\tilde{\mathbf{A}} \cdot \tilde{\mathbf{B}}$. The Figures 2a) and d) agrees qualitatively with results of Hawkes & Yeates (2019) (see, Fig.4c, there). It is found that the flux F_β is substantially smaller than the F_Ω . Also, in all the cases the net helicity flux from each bipolar region is close to zero.

3.2. Bipolar regions in the dynamo evolution.

We make a run of the dynamo model with the random injections of the bipolar regions by means of the magnetic buoyancy instability. The instability is randomly initiated in the northern or southern hemispheres, and the longitude, ϕ_0 , is also chosen randomly. We arbitrary chose the fluctuation interval $\tau_\beta = 0.01P$. After injection of the perturbation the evolution is solely determined by the dynamo equations. Note, that the condition of the buoyancy instability is defined by the critical magnetic field strength, see the Eq.(2.8).

Figure 3 shows the time-latitude diagrams for the toroidal magnetic field evolution, as well as , the small-scale helicity density, $\langle \chi \rangle$ and the helicity density fluxes F_Ω , F_α and F_β for axisymmetric and nonaxisymmetric magnetic field. The model shows the regular dynamo waves of the toroidal magnetic field which drifts toward equator in course of the magnetic cycle. The emerging bipolar regions show no effect on the butterfly diagram because the coupling between axisymmetric and nonaxisymmetric modes is weak. However, the bipolar regions have the cumulative effect on the rate of the magnetic flux loss. Therefore they affect the magnitude of the axisymmetric toroidal field. The properties of the given model was discussed in details by Pipin & Kosovichev

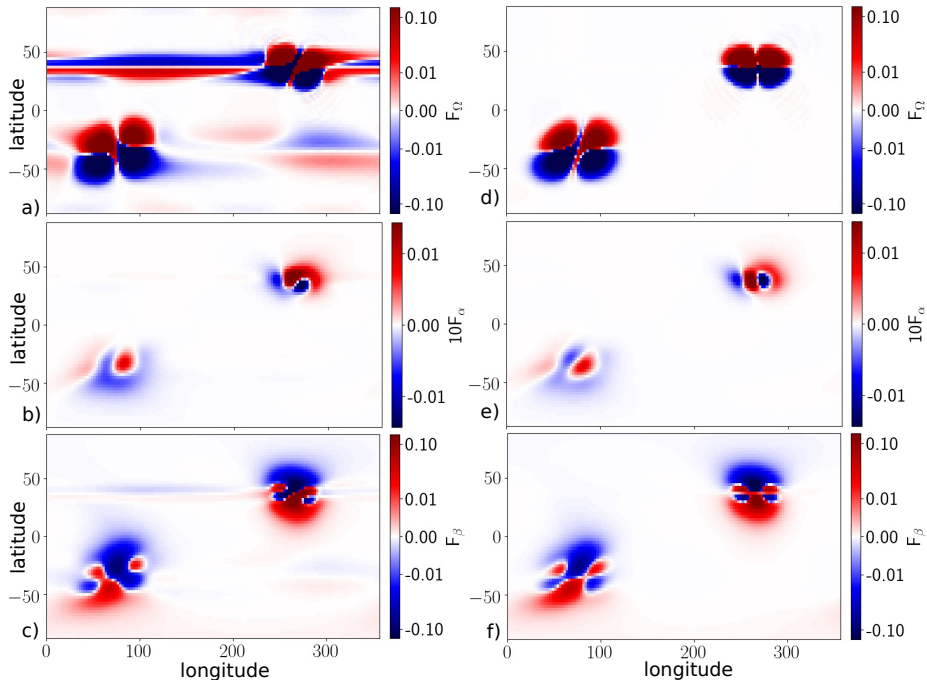


FIGURE 2. The helicity density fluxes, a) F_{Ω} - the flux due to differential rotation; b) the flux due the α - effect, F_{α} ; c) the flux due to the magnetic buoyancy, F_{β} ; the panels d), e) and f) shows the same for the model without tilt, i.e., $\alpha_{\beta} = 0$.

(2018). The small-scale helicity density, $\langle \chi \rangle$ evolves in following conservation law helicity density. This conservation law preserves the integral balance between $\langle \chi \rangle$, $\overline{\mathbf{A} \cdot \mathbf{B}}$ and $\overline{\tilde{\mathbf{A}} \cdot \tilde{\mathbf{B}}}$. In the quasi stationary state the $\overline{\mathbf{A} \cdot \mathbf{B}}$ contribution is much larger than $\overline{\tilde{\mathbf{A}} \cdot \tilde{\mathbf{B}}}$ (cf, Fig.5d). Therefore, the $\langle \chi \rangle$ evolution follows the standard hemispheric helicity rule.

The time-latitude variations of the, $\overline{\tilde{\mathbf{A}} \cdot \tilde{\mathbf{B}}} = \overline{\tilde{\chi}}$, show two bands in each hemisphere. The near equatorial bands show the positive sign in the northern hemisphere and the negative in the southern one. In the polar sides the situation is opposite. This patterns results naturally from the longitudinal averaging of the synoptic maps like that shown in Fig.1c. Interesting that in the run without tilt effect these bands show some equatorial drift, which results into noisy behavior of the $\overline{\tilde{\mathbf{A}} \cdot \tilde{\mathbf{B}}}$ near equator in that run. The time-latitude diagram of the $\overline{\tilde{\mathbf{A}} \cdot \tilde{\mathbf{B}}}$ shows sometimes the same sign of helicity on both hemispheres. This period correspond to the time when the wave of the toroidal magnetic field goes close to equator. Therefore there is interaction of the bipolar regions emerging in opposite hemispheres. The helicity fluxes due to the differential rotation are opposite for the axisymmetric and nonaxisymmetric magnetic field (see, Fig. 3b and e). Our results show that the helicity fluxes due to the mean-electromotive force effects are substantially less than those from effect of the differential rotation. The butterfly diagram of the F_{Ω} agrees qualitatively with results of Hawkes & Yeates (2019) (see, Fig.3c, there).

Figure 4 shows the integral parameters of the run. The total flux of the radial magnetic field can be considered as a proxy of the sunspot activity (Stenflo 2013). Beside the main magnetic cycle variation, this parameter shows a short-term quasi-biennial variations (see, Frick *et al.* 2020). In our model these oscillations follows evolution of the nonaxisymmetric magnetic field which are induced by the bipolar region formation.

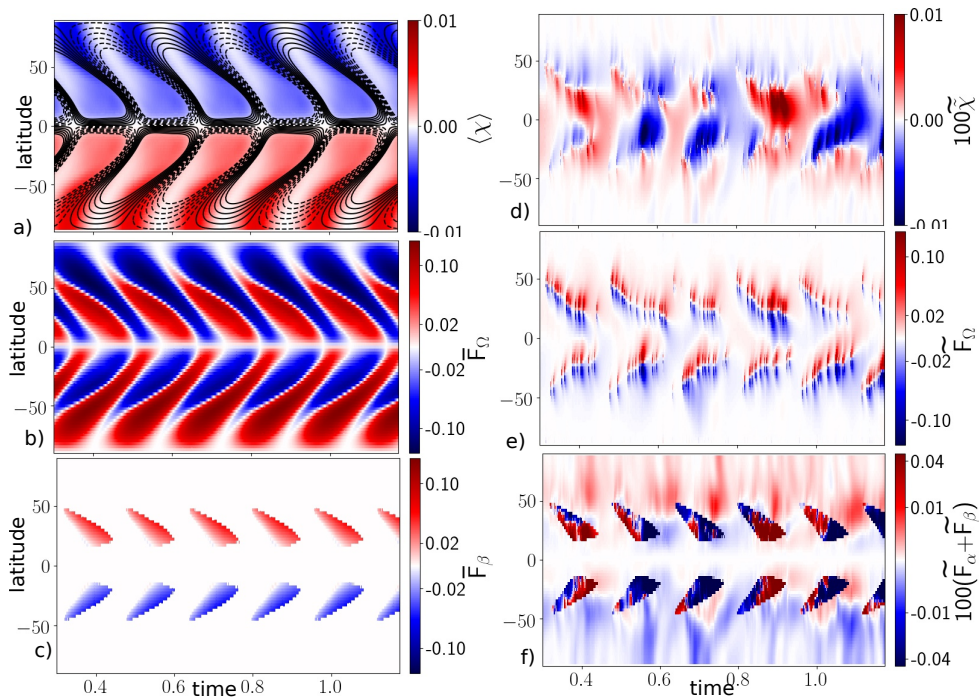


FIGURE 3. a) The time-latitude diagrams for the toroidal magnetic field (contours) and the small-scale helicity density, $\langle \chi \rangle$, is shown by the background image; b) the large-scale magnetic field helicity flux due to the differential rotation; c) the same as b) for the flux due to the magnetic buoyancy; d) the time-latitude evolution of the helicity density of the nonaxisymmetric magnetic field; e) show the same as b) for the helicity flux due to stretching of the nonaxisymmetric magnetic field due to the differential rotation flux; f) show the sum of the fluxes F_α and F_β for the nonaxisymmetric magnetic field.

The dynamo evolution of the axisymmetric and nonaxisymmetric magnetic field results in the opposite helicity fluxes by the differential rotation in the North and the South hemispheres. Note, the phase difference between variations of the sunspot proxy, \overline{F}_Ω and \overline{F}_β . Our results agree qualitatively with the solar observations (c.f., Berger & Ruzmaikin 2000; Zhang 2006).

Figure 5 shows snapshots of the magnetic field and the helicity density distributions for the period of maximum of the toroidal magnetic field cycle. The obtained magnetic field distribution is much simpler than the longitudinal structure of the solar activity proxies. This is likely because the range of the spatial scales which are involved in the dynamo model is at least factor 10 less than in the real Sun (see, Fig.10 in Pipin & Kosovichev 2018). Also, the dynamo model operates by the averaged equations, where, the effect of the small-scale flows is replaced by the mean electromotive force. The helicity patterns near the bipolar regions are qualitatively similar to the case shown in Fig.1b and not in Fig.1c. Note, that the Fig.5b shows the helicity density of the nonaxisymmetric magnetic field, $\overline{\mathbf{A}} \cdot \overline{\mathbf{B}}$. The interaction of the emerging bi-poles with the background large-scale nonaxisymmetric magnetic field produces the pattern similar to that in Fig.1b. At the right side of the snapshot we show the mean distribution of the $\overline{\chi}$, $\overline{\mathbf{A}} \cdot \overline{\mathbf{B}}$ and $\overline{\mathbf{A}} \cdot \overline{\mathbf{B}}$ for this synoptic map. We find that in the model the $\overline{\mathbf{A}} \cdot \overline{\mathbf{B}}$ has much less magnitude in compare with other two.

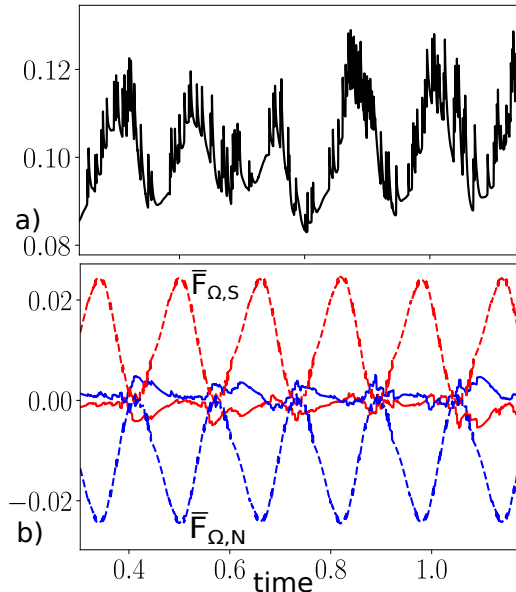


FIGURE 4. a) The total flux of the radial magnetic field; b) the axisymmetric (dashed lines) and nonaxisymmetric (solid lines) parts of the helicity fluxes from differential rotation, for the North and South hemispheres.

4. Discussion and conclusions

In the paper we study the effect of the emerging bipolar regions on the magnetic helicity density distributions and the helicity density fluxes. We employ a simplified dynamo model, which neglects the magnetic evolution in the radial direction. In the past, the models of surface dynamo waves were often used to illustrate the main principles and basic effects of a dynamo operating in the thin shear layer (Parker 1993; Moss *et al.* 2004, 2008). In earlier studies, it was found that the 1D models show the solar-type dynamo only for the certain range of the dynamo governing parameters. We extend our model from 1D axisymmetric to 2D nonaxisymmetric case in such a way that the model keeps the basic properties of the axisymmetric solar-type dynamo. Our formulation follows the framework of Moss *et al.* (2008) and contains results of their model in 1D limit. These restrictions result in the heuristic character of our model. Comparing our results with observations, we have to bear in mind that in the model the magnetic field dynamo generation and the bipolar region formation occur in the same place. The formation of the bipolar regions by means of the magnetic buoyancy instability is the main source of the nonaxisymmetric magnetic field in our model. After Parker (1984), the magnetic buoyancy instability is usually considered as a primary process in sunspot formation. In the mean-field model, this instability results in effective nonlinear pumping of the large-scale magnetic field outward in radial. Our model employs this instability in the heuristic way. Note, that the magnetic buoyancy instability is not the only mechanism which is capable to form the sunspots from the large-scale toroidal magnetic field (see, a review of Losada *et al.* 2017). Pipin & Kosovichev (2018) found that the model shows the spectral properties of the nonaxisymmetric magnetic field distribution in agreement with observations. They found that the large-scale nonaxisymmetric magnetic field results mainly from the diffusive decay of the bipolar regions.

In this paper our main goal was to find typical magnetic helicity patterns which we can observe on the surface of the Sun. We look to the case of the simple bipolar region

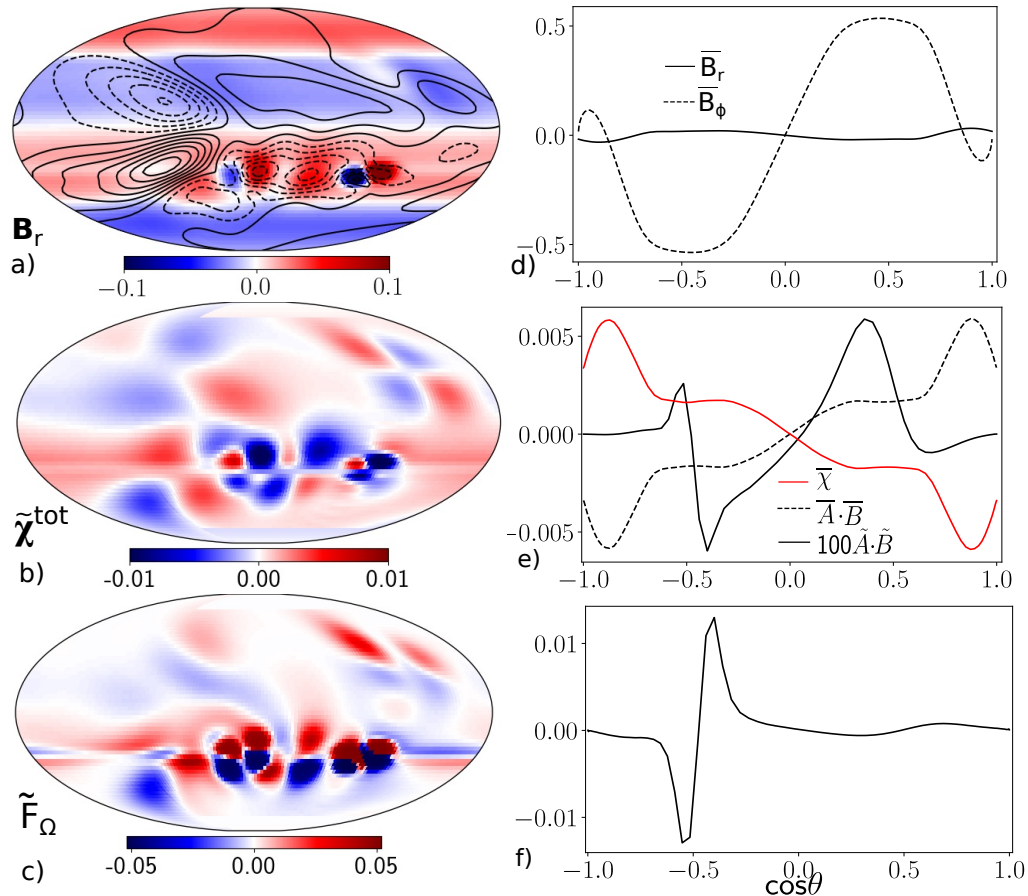


FIGURE 5. a) Snapshots of the radial magnetic field, $\langle B \rangle_r$, (color image) and the nonaxisymmetric toroidal field, \tilde{B}_ϕ , contours are shown in the same range as $\langle B \rangle_r$; b) the total helicity density of the nonaxisymmetric field, $\tilde{\chi}^{(tot)}$, (see, Eq.2.14); c) the snapshot of the helicity density flux due the differential rotation, \tilde{F}_Ω (nonaxisymmetric part); panels d),e) and f) show the mean latitudinal profiles of the magnetic field and helicity parameters. The snapshots are taken around the maximum of the toroidal magnetic field cycle, at the diffusive time ≈ 1 .

which is formed from the large-scale toroidal magnetic field by means of the magnetic buoyancy. We simulate the tilt in heuristic way using the nonlinear α_β -effect which is induced by the magnetic buoyancy instability. The origin of tilt is not specified. Such mechanisms was discussed in a number of papers (see, Leighton 1969; Ferriz-Mas *et al.* 1994; Fisher *et al.* 1999; Charbonneau 2011). We find that formation of the bipolar regions together with the large-scale magnetic field produce the quadrupole magnetic helicity density pattern (Figs1b,5c). The effect of the tilt in the bipolar region results in the tilt of the helicity pattern. The qualitatively similar results are found recently by Yeates (2020) using a completely different approach. Pipin *et al.* (2019) studied the helicity density distributions of the solar magnetic field using observations of the Helioseismic and Magnetic Imager (HMI, Scherrer *et al.* 2012) on board Solar Dynamics Observatory (SDO, Pesnell *et al.* 2012). The Figure 6 shows examples of the magnetic field and the magnetic helicity density synoptic maps for the Carrington rotation 2157. The two relatively small active regions in the southern hemisphere, A and B show the

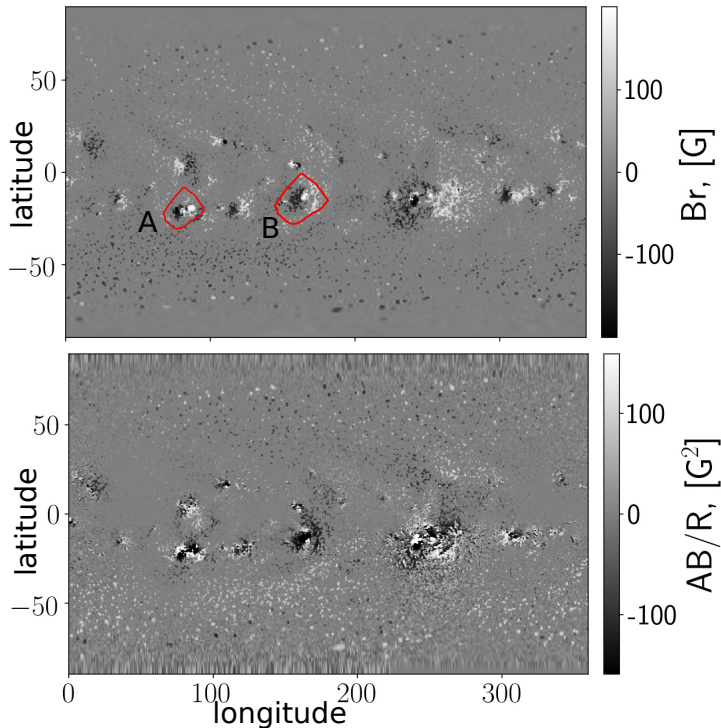


FIGURE 6. Synoptic maps of the radial magnetic field (top) and the magnetic helicity density (bottom) for the CR2157 (in following to results of Pipin *et al.* 2019).

quadrupole helicity density distributions in a qualitatively agreement with results of our study. The best agreement is for the region A. It is likely because it has a relatively simple distribution of the radial magnetic field flux.

In our model the dynamo process and the bipolar region formation occur in the same place. The emerging bipolar regions results in the loss of the magnetic field flux and quenching the large-scale dynamo. We find no a profound effect of these bi-poles on the helical properties of the dynamo. This is likely due to specific of our model. Despite, the nonlinear α_β effect produces some amount of the large-scale poloidal magnetic field flux (see, e.g., Fig1a), it does not affect much the background axisymmetric dynamo process. This is contrary to the assumptions of the Babcock-Leighton dynamo scenario (Cameron & Schüssler 2017). To satisfy this scenario we need a meridional circulation in the model. This probably requires the 3D model. Besides, it is likely that the large-scale dynamo, which utilizes such α_β effect acting on the nonaxisymmetric magnetic field, operates in the highly supercritical regimes (Ferriz-Mas *et al.* 1994). This is contrary to our original intention to have the solar-type dynamo model as a limit in 1D-case. Therefore, we can not expect a considerable effect of the generated $\overline{\mathbf{A} \cdot \mathbf{B}}$ on the small-scale helicity density evolution. The modeled $\langle \chi \rangle$ distributions are determined by the axisymmetric type of the dynamo model. The $\overline{\mathbf{A} \cdot \mathbf{B}}$ shows the inverted HHR near equator in compare the sign of the current helicity density of the solar active regions, (Zhang *et al.* 2010, 2016). The positive sign of the magnetic helicity density from tilted bipolar regions was anticipated in earlier studies (Pevtsov *et al.* 2014). Theoretically, it is expected that the tilt can results in the internal twist opposing to the writhe by the magnetic tensions (Blackman & Brandenburg 2003). In our model this process is taken into account by the conservation

law. Following to this law the small-scale helicity density $\bar{\chi}$ evolves in balance with the $\bar{\mathbf{A}} \cdot \bar{\mathbf{B}}$ helicity density of the axisymmetric field, $\bar{\mathbf{A}} \cdot \bar{\mathbf{B}}$. The heuristic type of our model do not allow a detailed quantitative comparison with observations. This can be improved in the 3D models, which allow to take into account all the dynamo effects in a physically consistent way. We may anticipate that for a shallow process of the sunspot formation, the 3D models can give the results which agrees qualitatively with ours.

Summing up, it is found the emerging bipolar regions produce the quadrupole helicity density patterns. The similar patterns were found for the helicity flux by means of the differential rotation. We find that the tilted bipolar regions show the inverted hemispheric helicity rule near equator in compare with observations of the magnetic helicity in the solar active regions. In general, our results suggest that on the intermediate scales such as the scale of the bipolar active regions the averaged magnetic helicity distribution can show no definite sign distribution in the northern and southern hemisphere of the Sun.

Acknowledgements The author acknowledge the financial support by the Russian Foundation for Basic Research grant 19-52-53045 and support of scientific project FR II.16 of ISTEP SB RAS. This work utilizes HMI data which are used here are courtesy of NASA/SDO and the HMI science teams. This work was borne out of discussions held among the authors during “Solar Helicities in Theory and Observations: Implications for Space Weather and Dynamo Theory” Program at Nordic Institute for Theoretical Physics (NORDITA) in 4–29 March 2019.

REFERENCES

- BAO, S. & ZHANG, H. 1998 Patterns of current helicity for the twenty-second solar. *ApJ* **496**, L43–L46. 1
- BERGER, MITCHELL A.; FIELD, G. B. 1984 The topological properties of magnetic helicity. *Journal of Fluid Mechanics* **147**. 1
- BERGER, M. A. & HORNIG, G. 2018 A generalized poloidal-toroidal decomposition and an absolute measure of helicity. *Journal of Physics A Mathematical General* **51**, 495501. 2, 5.3
- BERGER, M. A. & RUZMAIKIN, A. 2000 Rate of helicity production by solar rotation. *J. Geophys. Res.* **105**, 10481–10490. 1, 2, 3.2
- BLACKMAN, E. G. & BRANDENBURG, A. 2003 Doubly helical coronal ejections from dynamos and their role in sustaining the solar cycle. *ApJL* **584**, L99–L102, arXiv: astro-ph/0212010. 1, 2, 4
- BLACKMAN, E. G. & THOMAS, J. H. 2015 Explaining the observed relation between stellar activity and rotation. *MNRAS* **446**, L51–L55, arXiv: 1407.8500. 1
- BRANDENBURG, A. 2018 Advances in mean-field dynamo theory and applications to astrophysical turbulence. *Journal of Plasma Physics* **84**, 735840404. 2, 2
- BRANDENBURG, A., PETRIE, G. J. D. & SINGH, N. K. 2017 Two-scale analysis of solar magnetic helicity. *ApJ* **836**, 21. 1
- BRANDENBURG, A. & SUBRAMANIAN, K. 2005 Astrophysical magnetic fields and nonlinear dynamo theory. *Phys. Rep.* **417**, 1–209, arXiv: arXiv:astro-ph/0405052. 1, 2
- CAMERON, R. H. & SCHÜSSLER, M. 2017 Understanding solar cycle variability. *ApJ* **843**, 111, arXiv: 1705.10746. 4
- CHARBONNEAU, P. 2011 Dynamo models of the solar cycle. *Living Reviews in Solar Physics* **2**, 2. 2, 4
- FERRIZ-MAS, A., SCHMITT, D. & SCHUESSLER, M. 1994 A dynamo effect due to instability of magnetic flux tubes. *A & A* **289**, 949–956. 4, 4
- FISHER, G. H., LONGCOPE, D. W., LINTON, M. G., FAN, Y. & PEVTSOV, A. A. 1999 The origin and role of twist in active regions. In *Stellar Dynamos: Nonlinearity and Chaotic Flows* (ed. M. Nunez & A. Ferriz-Mas), *Astronomical Society of the Pacific Conference Series*, vol. 178, p. 35. 4
- FRICK, P., SOKOLOFF, D., STEPANOV, R., PIPIN, V. & USOSKIN, I. 2020 Spectral characteristic

- of mid-term quasi-periodicities in sunspot data. *MNRAS* **491** (4), 5572–5578, arXiv: 1911.06881. 3.2
- HAWKES, G. & YEATES, A. R. 2019 Hemispheric injection of magnetic helicity by surface flux transport. *A & A* **631**, A138. 1, 3.1, 3.2
- HUBBARD, A. & BRANDENBURG, A. 2012 Catastrophic quenching in $\alpha\Omega$ dynamos revisited. *ApJ* **748**, 51, arXiv: 1107.0238. 2
- JENNINGS, R., BRANDENBURG, A., TUOMINEN, I. & MOSS, D. 1990 Can stellar dynamos be modelled in less than three dimensions? *A & A* **230**, 463–473. 2
- KITCHATINOV, L. L. & PIPIN, V. V. 1993 Mean-field buoyancy. *A & A* **274**, 647–652. 2, 2
- KLEEORIN, N., MOSS, D., ROGACHEVSKII, I. & SOKOLOFF, D. 2000 Helicity balance and steady-state strength of the dynamo generated galactic magnetic field. *A & A* **361**, L5–L8, arXiv: arXiv:astro-ph/0205266. 2
- KLEEORIN, N. & ROGACHEVSKII, I. 1999 Magnetic helicity tensor for an anisotropic turbulence. *Phys. Rev.E* **59**, 6724–6729. 2, 2
- KLEEORIN, N. I. & RUZMAIKIN, A. A. 1982 Dynamics of the average turbulent helicity in a magnetic field. *Magnetohydrodynamics* **18**, 116–122. 2, 2
- KRAUSE, F. & RÄDLER, K.-H. 1980 *Mean-Field Magnetohydrodynamics and Dynamo Theory*. Berlin: Akademie-Verlag. 2, 2, 2, 5.1, 5.1
- LEIGHTON, R. B. 1969 A Magneto-Kinematic Model of the Solar Cycle. *ApJ* **156**, 1. 4
- LOSADA, I. R., WARNECKE, J., GLOGOWSKI, K., ROTH, M., BRANDENBURG, A., KLEEORIN, N. & ROGACHEVSKII, I. 2017 A new look at sunspot formation using theory and observations. In *Fine Structure and Dynamics of the Solar Atmosphere* (ed. S. Vargas Domínguez, A. G. Kosovichev, P. Antolin & L. Harra), *IAU Symposium*, vol. 327, pp. 46–59, arXiv: 1704.04062. 4
- MACKAY, D. H. & YEATES, A. R. 2012 The sun’s global photospheric and coronal magnetic fields: Observations and models. *Living Reviews in Solar Physics* **9**, 6, arXiv: 1211.6545. 1
- MITRA, D., CANDELARESI, S., CHATTERJEE, P., TAVAKOL, R. & BRANDENBURG, A. 2010 Equatorial magnetic helicity flux in simulations with different gauges. *Astronomische Nachrichten* **331**, 130, arXiv: 0911.0969. 2
- MOFFATT, H. K. 1978 *Magnetic Field Generation in Electrically Conducting Fluids*. Cambridge, England: Cambridge University Press. 2
- MOSS, D., SOKOLOFF, D., KUZANYAN, K. & PETROV, A. 2004 Stellar dynamo waves: Asymptotic configurations. *Geophysical and Astrophysical Fluid Dynamics* **98**, 257–272. 4
- MOSS, D., SOKOLOFF, D., USOSKIN, I. & TUTUBALIN, V. 2008 Solar grand minima and random fluctuations in dynamo parameters. *Solar Phys.* **250**, 221–234. 2, 2, 4, 5.2
- NOYES, R. W., WEISS, N. O. & VAUGHAN, A. H. 1984 The relation between stellar rotation rate and activity cycle periods. *ApJ* **287**, 769–773. 2
- PARKER, E. N. 1984 Magnetic buoyancy and the escape of magnetic fields from stars. *ApJ* **281**, 839–845. 2, 4
- PARKER, E. N. 1993 A solar dynamo surface wave at the interface between convection and nonuniform rotation. *ApJ* **408**, 707–719. 4
- PESNELL, W. D., THOMPSON, B. J. & CHAMBERLIN, P. C. 2012 The solar dynamics observatory (sdo). *Sol.Phys.* **275**, 3–15. 4
- PEVTSOV, A. A., BERGER, M. A., NINDOS, A., NORTON, A. A. & VAN DRIEL-GESZTELYI, L. 2014 Magnetic helicity, tilt, and twist. *Space Sci. Rev.* **186**, 285–324. 4
- PEVTSOV, A. A., CANFIELD, R. C. & METCALF, T. R. 1994 Patterns of helicity in solar active regions. *ApJL* **425**, L117–L119. 1
- PIPIN, V. 2018 Vvpipin/2dspdy 0.1.1. 2
- PIPIN, V. V. & KOSOVICHEV, A. G. 2018 Does nonaxisymmetric dynamo operate in the sun? *ArXiv e-prints* p. arXiv:1808.05332, arXiv: 1808.05332. 1, 2, 2, 2, 3.2, 3.2, 4
- PIPIN, V. V. & PEVTSOV, A. A. 2014 Magnetic helicity of the global field in solar cycles 23 and 24. *ApJ* **789**, 21, arXiv: 1402.2386. 5.1
- PIPIN, V. V., PEVTSOV, A. A., LIU, Y. & KOSOVICHEV, A. G. 2019 Evolution of magnetic helicity in solar cycle 24. *ApJ* **877** (2), L36, arXiv: 1905.00772. 1, 4, 6

- PIPIN, V. V., SOKOLOFF, D. D., ZHANG, H. & KUZANYAN, K. M. 2013 Helicity conservation in nonlinear mean-field solar dynamo. *ApJ* **768**, 46, arXiv: 1211.2420. 2, 2
- POUQUET, A., FRISCH, U. & LÉORAT, J. 1975 Strong MHD helical turbulence and the nonlinear dynamo effect. *J. Fluid Mech.* **68**, 769–778. 1, 2
- RÜDIGER, G., KITCHATINOV, L. L. & BRANDENBURG, A. 2011 Cross helicity and turbulent magnetic diffusivity in the solar convection zone. *Sol.Phys.* **269**, 3–12, arXiv: 1004.4881. 2
- RUEDIGER, G. & KICHATINOV, L. L. 1993 Alpha-effect and alpha-quenching. *A & A* **269** (1-2), 581–588. 2
- SCHERRER, P. H., SCHOU, J., BUSH, R. I., KOSOVICHEV, A. G., BOGART, R. S., HOEKSEMA, J. T., LIU, Y., DUVAL, T. L., ZHAO, J., TITLE, A. M., SCHRIJVER, C. J., TARBELL, T. D. & TOMCZYK, S. 2012 The helioseismic and magnetic imager (hmi) investigation for the solar dynamics observatory (sdo). *Sol.Phys.* **275**, 207–227. 4
- SEEHAFER, N. 1994 Alpha effect in the solar atmosphere. *A & A* **284**, 593–598. 1
- SINGH, N. K., KÄPYLÄ, M. J., BRANDENBURG, A., KÄPYLÄ, PETRI, J., LAGG, A. & VIRTANEN, I. 2018 Bihelical spectrum of solar magnetic helicity and its evolution. *ApJ* **863**, 182, arXiv: 1804.04994. 1
- STENFLO, J. O. 2013 Solar magnetic fields as revealed by stokes polarimetry. *Astron. & Astrophys. Rev.* **21**, 66, arXiv: 1309.5454. 1, 3.2
- TLATOV, A., ILLARIONOV, E., SOKOLOFF, D. & PIPIN, V. 2013 A new dynamo pattern revealed by the tilt angle of bipolar sunspot groups. *MNRAS* **432** (4), 2975–2984, arXiv: 1302.2715. 2
- TORIUMI, S. & WANG, H. 2019 Flare-productive active regions. *Living Reviews in Solar Physics* **16** (1), 3, arXiv: 1904.12027. 2
- YEATES, A. R. 2020 The Minimal Helicity of Solar Coronal Magnetic Fields. *ApJL* **898** (2), L49, arXiv: 2007.10649. 4
- ZHANG, H., BRANDENBURG, A. & SOKOLOFF, D. D. 2016 Evolution of magnetic helicity and energy spectra of solar active regions. *ApJ* **819**, 146. 4
- ZHANG, H., SAKURAI, T., PEVTSOV, A., GAO, Y., XU, H., SOKOLOFF, D. D. & KUZANYAN, K. 2010 A new dynamo pattern revealed by solar helical magnetic fields. *MNRAS* **402**, L30–L33, arXiv: 0911.5713. 1, 4
- ZHANG, M. 2006 Helicity observations of weak and strong fields. *ApJL* **646**, L85–L88, arXiv: astro-ph/0606231. 3.2

5. Appendix

5.1. The large-scale magnetic field and its vector potential

We decompose the total magnetic field induction vector on the sum of the axisymmetric and non-axisymmetric parts: $\langle \mathbf{B} \rangle = \bar{\mathbf{B}} + \tilde{\mathbf{B}}$. In the spherical coordinates, the axisymmetric part, $\bar{\mathbf{B}}$, is represented as follows:

$$\begin{aligned} \bar{\mathbf{B}} &= \hat{\phi}B + \nabla \times (A\hat{\theta}) \\ &= \hat{\phi}B - \frac{\hat{r}}{r} \frac{\partial A \sin \theta}{\partial \mu} - \frac{\hat{\theta}}{r} \frac{\partial rA}{\partial r}, \end{aligned} \quad (5.1)$$

where, \hat{r} is the unit vector in the radial direction, $\hat{\theta}$ is the unit vector in meridional direction, and $\hat{\phi}$ is the unit vector in the azimuthal direction, $\mu = \cos \theta$. In this paper we assume that the scalars A and B are independent of radius. Therefore, for the axisymmetric magnetic field at $r = R$ we get

$$\bar{\mathbf{B}} = \hat{\phi}B - \frac{\hat{r}}{R} \frac{\partial A \sin \theta}{\partial \mu} - \frac{\hat{\theta}A}{R}. \quad (5.2)$$

The above definitions preserve the divergency free vector-field, $\nabla \cdot \bar{\mathbf{B}} = 0$. For the axisymmetric part of the vector potential we have

$$\bar{\mathbf{A}} = \hat{r}A_r + \hat{\phi}A, \quad (5.3)$$

where $B = \partial A_r / \partial \mu$ (see, Pipin & Pevtsov 2014). The unique axisymmetric potential is found for the gauge $\int_{-1}^1 A_r d\mu = 0$ (cf., below derivations). For the nonaxisymmetric part of magnetic field, we use the same idea. In following Krause & Rädler (1980), we write:

$$\begin{aligned} \tilde{\mathbf{B}} &= \nabla \times (\hat{r}T) + \nabla \times \nabla \times (\hat{r}S) \\ &= -\frac{\hat{r}}{r}\Delta_\Omega S + \hat{\theta} \left(\frac{1}{\sin\theta} \frac{\partial T}{\partial \phi} - \frac{\sin\theta}{r} \frac{\partial}{\partial \mu} \frac{\partial rS}{\partial r} \right) + \hat{\phi} \left(\sin\theta \frac{\partial T}{\partial \mu} + \frac{1}{r \sin\theta} \frac{\partial}{\partial \phi} \frac{\partial rS}{\partial r} \right). \end{aligned} \quad (5.4)$$

Besides, we apply the following gauge (see, e.g., Krause & Rädler 1980):

$$\int_0^{2\pi} \int_{-1}^1 S d\mu d\phi = \int_0^{2\pi} \int_{-1}^1 T d\mu d\phi = 0. \quad (5.5)$$

Assuming that the potential's scalar functions S and T are independent of the radius, we get,

$$\tilde{\mathbf{B}} = -\frac{\hat{r}}{R}\Delta_\Omega S + \hat{\theta} \left(\frac{1}{\sin\theta} \frac{\partial T}{\partial \phi} - \frac{\sin\theta}{R} \frac{\partial S}{\partial \mu} \right) + \hat{\phi} \left(\sin\theta \frac{\partial T}{\partial \mu} + \frac{1}{R \sin\theta} \frac{\partial S}{\partial \phi} \right), \quad (5.6)$$

and $\nabla \cdot \tilde{\mathbf{B}} = 0$. With the above assumptions, the nonaxisymmetric part of the vector-potential reads,

$$\begin{aligned} \tilde{\mathbf{A}} &= \hat{r}T + \nabla \times (\hat{r}S) \\ &= \hat{r}T + \frac{\hat{\theta}}{R \sin\theta} \frac{\partial S}{\partial \phi} + \hat{\phi} \frac{\sin\theta}{R} \frac{\partial S}{\partial \mu}. \end{aligned} \quad (5.7)$$

5.2. Dynamo equations

Applying these simplifications to Eq (2.1) and Eqs (2.2-2.4) we obtain the following set of dynamo equations in terms of the scalar functions, A, B, S , and T :

$$\partial_t B = -\sin\theta \frac{\partial \Omega}{\partial r} \frac{\partial}{\partial \mu} (\sin\theta A) + \eta_T \frac{\sin^2\theta}{R^2} \frac{\partial^2 (\sin\theta B)}{\partial \mu^2} \quad (5.8)$$

$$\begin{aligned} &+ \frac{\sin\theta}{R} \frac{\partial}{\partial \mu} \alpha \mu \langle B_r \rangle + \frac{\alpha \mu}{R} \langle B_\theta \rangle \\ &- \frac{1}{R} V_\beta \langle B_\phi \rangle - \frac{B}{\tau} \end{aligned} \quad (5.9)$$

$$\partial_t A = \alpha \mu \langle B_\phi \rangle + \eta_T \frac{\sin^2\theta}{R^2} \frac{\partial^2 (\sin\theta A)}{\partial \mu^2} - \frac{V_\beta}{R} A - \frac{A}{\tau}, \quad (5.10)$$

$$\partial_t \Delta_\Omega T = -\Delta_\Omega \delta \Omega \frac{\partial T}{\partial \phi} + \frac{\eta_T}{R^2} \Delta_\Omega^2 T \quad (5.11)$$

$$\begin{aligned} &- \frac{1}{R} \frac{\partial \Omega}{\partial r} \sin^2\theta \frac{\partial \Delta_\Omega S}{\partial \mu} - \frac{1}{R} \frac{\partial}{\partial \phi} \left[\frac{\alpha + \alpha_\beta}{\sin\theta} \mu \langle B_\phi \rangle \right] \\ &+ \Delta_\Omega \frac{\alpha \mu}{R} (\langle B_r \rangle \sin^2\theta + \mu \sin\theta \langle B_\theta \rangle) \end{aligned} \quad (5.12)$$

$$\begin{aligned}
& + \frac{1}{R} \frac{\partial}{\partial \mu} \alpha \mu \sin \theta \{ \mu \sin \theta \langle B_r \rangle + \mu^2 \langle B_\theta \rangle \} \\
& - \frac{1}{R \sin \theta} \frac{\partial}{\partial \phi} \langle B_\theta \rangle V_\beta - \frac{\partial}{\partial \mu} (\sin \theta \langle B_\phi \rangle V_\beta),
\end{aligned}$$

$$\partial_t \Delta_\Omega S = - \left(\delta \Omega \Delta_\Omega \frac{\partial}{\partial \phi} S \right) + \frac{\eta_T}{R^2} \Delta_\Omega^2 S \quad (5.13)$$

$$+ \frac{\partial}{\partial \mu} (\alpha + \alpha_\beta) \mu \sin \theta \langle B_\phi \rangle \quad (5.14)$$

$$\begin{aligned}
& + \frac{\partial}{\partial \phi} \left\{ \frac{\alpha \mu}{\sin \theta} (\langle B_\theta \rangle + \sin \theta (\mathbf{e} \cdot \langle \mathbf{B} \rangle)) \right\} \\
& - \frac{1}{\sin \theta} \frac{\partial}{\partial \phi} (\langle B_\phi \rangle V_\beta) + \frac{\partial}{\partial \mu} (\sin \theta \langle B_\theta \rangle V_\beta),
\end{aligned}$$

where $\Delta_\Omega = \frac{\partial}{\partial \mu} \sin^2 \theta \frac{\partial}{\partial \mu} + \frac{1}{\sin^2 \theta} \frac{\partial^2}{\partial \phi^2}$ and $\mu = \cos \theta$. To simulate stretching of nonaxisymmetric magnetic field by the surface differential rotation we consider the latitudinal dependence of angular velocity $\delta \Omega = -0.25 \sin^2 \theta \Omega$ in Eqs (5.11) and (5.13), which are written in the coordinate system rotating with angular velocity Ω . The τ -terms in Eqs(5.8,5.10) were suggested by Moss *et al.* (2008) to account for turbulent diffusion in radial direction. Similarly to the cited paper we put $\tau = 3 \frac{R^2}{\eta_T}$.

5.3. Helicity evolution equation

We start from the mean-field evolution equations for the large-scale magnetic field:

$$\partial_t \langle \mathbf{B} \rangle = \nabla \times (\mathcal{E} + \langle \mathbf{U} \rangle \times \langle \mathbf{B} \rangle - \eta \nabla \times \langle \mathbf{B} \rangle) \quad (5.15)$$

For the time derivative of the magnetic helicity of the large-scale field in a volume we get,

$$\begin{aligned}
\frac{d}{dt} \int \langle \mathbf{A} \rangle \cdot \langle \mathbf{B} \rangle dV & = \int (\langle \mathbf{A} \rangle \cdot \partial_t \langle \mathbf{B} \rangle + \langle \mathbf{B} \rangle \cdot \partial_t \langle \mathbf{A} \rangle + \nabla \cdot \langle \mathbf{U} \rangle (\langle \mathbf{A} \rangle \cdot \langle \mathbf{B} \rangle)) \\
& = \int \{ 2 \langle \mathbf{A} \rangle \cdot \partial_t \langle \mathbf{B} \rangle + \nabla \cdot \langle \mathbf{U} \rangle (\langle \mathbf{A} \rangle \cdot \langle \mathbf{B} \rangle) \} dV + \oint (\langle \mathbf{A} \rangle \times \partial_t \langle \mathbf{A} \rangle) \cdot \mathbf{n} dS
\end{aligned} \quad (5.16)$$

Using the mean-field evolution equation we obtain:

$$\begin{aligned}
\frac{d}{dt} \int \langle \mathbf{A} \rangle \cdot \langle \mathbf{B} \rangle dV & = 2 \int (\mathcal{E} \cdot \langle \mathbf{B} \rangle - \eta \langle \mathbf{J} \rangle \cdot \langle \mathbf{B} \rangle) dV \\
& + 2 \int \nabla \cdot (\mathcal{E} \times \langle \mathbf{A} \rangle + \langle \mathbf{B} \rangle (\langle \mathbf{A} \rangle \cdot \langle \mathbf{U} \rangle) - \eta \langle \mathbf{J} \rangle \times \langle \mathbf{A} \rangle) dV \\
& - \oint (\langle \mathbf{A} \rangle \cdot \langle \mathbf{B} \rangle) (\langle \mathbf{U} \rangle \cdot \mathbf{n}) dS + \oint (\langle \mathbf{A} \rangle \times \partial_t \langle \mathbf{A} \rangle) \cdot \mathbf{n} dS,
\end{aligned} \quad (5.17)$$

where we denote $\langle \mathbf{J} \rangle = \nabla \times \langle \mathbf{B} \rangle$. In following the Eq.(2.12), the integral conservation law for the total helicity, $\langle \chi \rangle^{(tot)} = \langle \chi \rangle + \langle \mathbf{A} \rangle \cdot \langle \mathbf{B} \rangle$, evolution is

$$\frac{d}{dt} \int (\langle \chi \rangle + \langle \mathbf{A} \rangle \cdot \langle \mathbf{B} \rangle) dV = - \frac{1}{R_m \tau_c} \int \langle \chi \rangle dV - 2\eta \int \langle \mathbf{B} \rangle \cdot \langle \mathbf{J} \rangle dV - \int \nabla \cdot \mathcal{F}^\chi dV. \quad (5.18)$$

Subtracting, the Eq(5.17) from Eq(5.18) we get,

$$\begin{aligned}
\left(\frac{d}{dt} + \frac{1}{R_m \tau_c}\right) \int \langle \chi \rangle dV &= -2 \int \boldsymbol{\mathcal{E}} \cdot \langle \mathbf{B} \rangle dV - \int \boldsymbol{\nabla} \cdot \boldsymbol{\mathcal{F}}^\chi dV & (5.19) \\
&- 2 \oint (\boldsymbol{\mathcal{E}} \times \langle \mathbf{A} \rangle) \cdot \mathbf{n} dS - 2 \oint (\langle \mathbf{A} \rangle \cdot \langle \mathbf{U} \rangle) (\langle \mathbf{B} \rangle \cdot \mathbf{n}) dS \\
&- 2\eta \oint (\langle \mathbf{A} \rangle \times \langle \mathbf{J} \rangle) \cdot \mathbf{n} dS + \oint (\langle \mathbf{A} \rangle \cdot \langle \mathbf{B} \rangle) (\langle \mathbf{U} \rangle \cdot \mathbf{n}) dS \\
&- \oint (\langle \mathbf{A} \rangle \times \partial_t \langle \mathbf{A} \rangle) \cdot \mathbf{n} dS, & (5.20)
\end{aligned}$$

The last term, in the above equation, gets zero for a divergency free on the surface vector potentials (Berger & Hornig 2018). In our definitions, the vector potential is consisted of a sum of the divergency-free components and the pure radial components (see, the Eqs.(5.3,5.4)). Therefore the last term in the equation 5.19 is zero, as well.